Hindawi
Mathematical Problems in Engineering
Volume 2018, Article ID 9230609, 8 pages
https://doi.org/10.1155/2018/9230609

Research Article

The Elastic Solution of a Radial Heterogeneous Cylinder Subjected to Non-Uniform Distributed Normal and Tangential Loads

Wen Zhang

State Key Laboratory for Geomechanics and Deep Underground Engineering, China University of Mining and Technology, Xuzhou 221116, China

Correspondence should be addressed to Wen Zhang; zhangwen77@126.com

Received 11 January 2018; Revised 8 April 2018; Accepted 7 May 2018; Published 27 June 2018

Academic Editor: Seungik Baek

This paper presents an investigation of a cylinder with material attributes that vary arbitrarily in the radial direction under non-uniformly distributed normal and tangential pressures. A stress and displacement solution method for plane strain on a radial heterogeneous cylinder with inner and outer surfaces subjected to uneven normal and tangential pressures under two types of contact conditions (i.e., complete contact and smooth contact) is proposed based on the theory of elastic mechanics. In addition, a group of linear equations is derived, through which the analytical solution of a radial heterogeneous cylinder under a non-uniform load can be obtained. The validity of the analytical solution is verified by comparing it with the results of a numerical simulation. This research shows that the solution is more convenient and universal than traditional methods and can provide a theoretical basis for the stress state analysis, stability evaluation, and structure design of heterogeneous cylindrical structures, all of which have great significance in practical engineering.

1. Introduction

Cylinders are important structures that are widely used in civil and mining engineering in addition to other engineering fields, and they are commonly implemented in machinery and national defense applications. Therefore, research on the stress and deformation of cylinders in their applications (e.g., for shaft linings and tunnels) has important value for cylinder design and safety evaluations.

Cylinders subjected to uniform loads have been studied from many perspectives. The earliest known research on such cylinders produced the Lamé solution [1], which characterizes the stresses and deformation of elastic homogeneous cylinders under both internal and external uniform pressures; consequently, the Lamé solution has been widely utilized for cylinder design [2, 3]. In addition, numerous types of cylinders, including multilayer cylinders [4–6] and cylinders made of composite materials [7], particularly functional gradient cylinders [8], have been developed to cope with extreme working conditions (e.g., high temperatures, high pressures, and corrosion) [9, 10]. Shi [11] obtained the exact solution for N-layer elastic cylinders and cylinders comprising functional gradient materials by deriving a hypergeometric function. Furthermore, Sollund [12] established a group of recursive formulas and obtained the stress and deformation solution of N-layer cylinders under the joint action of uniform pressure and temperature loads. Horgan [13] performed a mechanical analysis of a functional gradient cylinder with an elastic modulus that radially varied as a power function under internal and external pressures and discussed the differences in the stress distributions between the actions of both the internal and external pressures. In addition, Lu [14] conducted an inversion analysis of a functionally graded material cylinder under the assumption that the stress state at every point on the cylinder was either $\sigma_\theta = c_1$ or $\sigma_\theta - \sigma_r = c_2$ and consequently developed an analytical solution for Young's modulus that varies with the radius.

However, most cylinders in practical engineering applications are subjected to non-axisymmetric loads. For instance,

shaft linings and shield tunnel linings experience non-axisymmetric loads due to variations in geological conditions and construction technologies. Uneven pressures can lead to tensile stresses in linings that are very dangerous for concrete structures [15–21]. For example, oil well casings installed within salt rock and mudstone are more prone to instabilities and loose bearing capacities as a consequence of rock creep than to the external water pressure because rock creep applies a non-uniform load to the casing [22–24]. In addition, the Couette flow of a viscous fluid between two cylinders applies non-uniform normal and tangential pressures on their surfaces. Therefore, it is necessary to analyze the stress and deformation of cylindrical structures under non-uniform loads. Some textbooks and related studies have provided analytical solutions for elastic homogeneous cylinders under non-uniform loads [25, 26], but little research has been performed on inhomogeneous cylinders. For example, Greenberg [27] investigated the static buckling of orthotropic composite cylindrical shells subjected to circumferentially non-uniform loads based on Flugge-type field equations. Furthermore, by assuming that the elastic modulus and the coefficient of thermal expansion are both power functions with radial coordinates, Jabbari analyzed a linear thermoelastic problem involving a functionally graded cylinder subjected to an internal non-uniform load. Rad [28] analyzed the two-dimensional steady-state thermal stresses on a hollow, thick cylinder made of functionally graded materials and obtained a semianalytical solution. Alternatively, Liew [29] divided a functional gradient cylinder into a number of thin homogeneous cylinders and employed the semi-inverse method to derive a solution for the thermal stresses on functional gradient cylinders under a non-uniform load that varies in circular coordinates. Batra [30] obtained the analytical solution for an incompressible functional gradient eccentric cylinder subjected to a non-uniform load and analyzed the stress and deformation variations with changes in the shear modulus according to a power function and an exponential function in the radial direction. Moreover, Li [31] determined the stress and displacement fields for a cylinder with mechanical parameters that arbitrarily changed in the radial direction under a non-uniform radial load using the theory of complex functions.

The above-mentioned analytical solutions have achieved notable progress; however, those solutions are excessively complex and do not consider the comprehensive effects of different loads. Therefore, this paper proposes a mechanical model of a radial heterogeneous cylinder subjected to a new type of non-uniform load. The stress and displacement solution of the model is deduced in consideration of the contact conditions between osculant layers (complete contact and smooth contact) using elastic mechanics. In this paper, $\widehat{\sigma}$ denotes the stress; $\widehat{u}$ and $\widehat{v}$ are the radial displacement and circumferential displacement, respectively; the subscripts r, θ and $r\theta$ represent the radial, circumferential, and shearing components, respectively; and the subscript i (i=1, 2, 3, …, n; as below) indicates the number of the layers in the cylinder.

2. Mechanical Model

2.1. Nondimensionalization of Parameters. To generalize the solution, we select appropriate normalized variables to transform the parameters into dimensionless forms. Regular variables with units are expressed with a ∧ symbol.

The load $\widehat{p}_a$ is used to scale the relevant stress and pressure, and the inner radius $\widehat{r}_i$ of each layer is used to scale the displacement. The load $\widehat{p}_a$ is selected according to the conditions of different problems. For example, the vertical stress at the distal end of the formation $\widehat{p}_a$ is obtained by analyzing the shaft well or the tunnel lining.

$p = \widehat{p}/\widehat{p}_a$ and $q = \widehat{q}/\widehat{p}_a$ are the dimensionless loads.

$\sigma_{ri} = \widehat{\sigma}_{ri}/\widehat{p}_a$, $\sigma_{\theta i} = \widehat{\sigma}_{\theta i}/\widehat{p}_a$, and $\sigma_{r\theta i} = \widehat{\sigma}_{r\theta i}/\widehat{p}_a$ represent the dimensionless forms of the stresses, and $G_i = \widehat{G}_i/\widehat{p}_a$ represents the dimensionless form of the shear modulus $\widehat{G}_i$.

$u_i = \widehat{u}_i/\widehat{r}_i$ and $v_i = \widehat{v}_i/\widehat{r}_i$ are the dimensionless displacements.

$\rho_i = (\widehat{r}/\widehat{r}_i)$ $(\widehat{r}_i \le \widehat{r} \le \widehat{r}_{i+1})$ and $r = (\widehat{r}/\widehat{r}_1)$ $(\widehat{r}_1 \le \widehat{r} \le \widehat{r}_{n+1})$ are nondimensional coordinates.

2.2. Mechanical Model. The pressure acting on the external cylinder can be expressed using a Fourier series dependent on the circumferential coordinates.

$$p(\theta) = \delta_0 + \sum_{t=1}^{\infty} \left[\xi_t \cos(t\theta) + \overline{\xi}_t \sin(t\theta)\right]$$
$$q(\theta) = \omega_0 + \sum_{t=1}^{\infty} \left[\omega_t \sin(t\theta) + \overline{\omega}_t \cos(t\theta)\right] \quad (1)$$

This study focuses on both δ parameter, which represents the uniform force that is self-balanced since the resulting value along the circumference is zero, and the cosine term, which is examined because of the similarity between the sine and cosine terms in the above equation. Moreover, the cosine terms are different; through analysis, the cosine term is self-balanced when $t \ge 2$, but the cosine term cannot balance itself when $t = 1$. Therefore, the distribution of the non-uniform load on the external cylinder is expressed as follows:

$$p = \delta + \xi \cos 2\theta \quad (2)$$

$$q = \omega \sin 2\theta \quad (3)$$

where p and q reflect the non-uniform distributed normal load and tangential load, respectively, and δ, ξ, and ω are the uniform and non-uniform distributed normal loads and the uneven tangential load, respectively. The tensile stress and outward radial displacement are positive according to the sign convention shown in Figure 1.

Figure 1 illustrates a force model of a radially inhomogeneous cylinder subjected to loads p and q. The radially inhomogeneous cylinder is regarded as an n-layered cylinder composed of several homogeneous and isotropically linear elastic layers. The inner and outer radii of the ith layer are r_i and r_{i+1}, respectively. The elastic modulus and Poisson's ratio are E_i and μ_i, respectively. The loads on the inner and outer surfaces are $p_i = \delta_i + \xi_i \cos 2\theta$ and $q_i = \omega_i \sin 2\theta$ and $p_{i+1} = \delta_{i+1} + \xi_{i+1} \cos 2\theta$ and $q_{i+1} = \omega_{i+1} \sin 2\theta$, respectively.

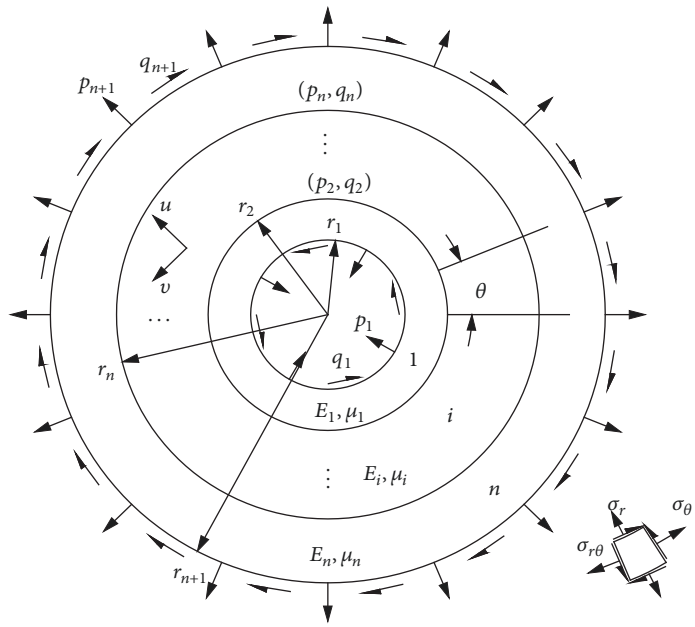

Figure 1: Mechanical model I: radially layered model.

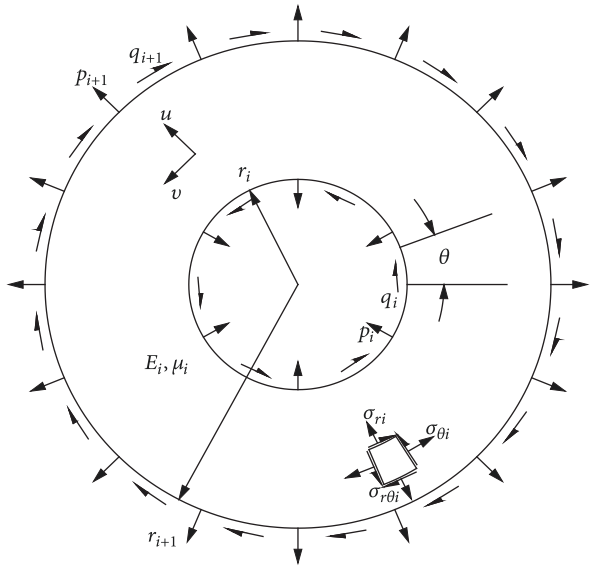

Figure 2: Single-layer model.

3. Model Solution

3.1. Single-Layer Model Solution. Mechanical model I can be decomposed into many single-layer models (see Figure 2).

The analytic solution of the single-layer model is given as follows [15–17]:

$$\begin{aligned} \sigma_{ri} &= h_{ri}(\rho_i) + g_{ri}(\rho_i) \cdot \cos 2\theta \\ h_{ri}(\rho_i) &= 2a_i + b_i\rho_i^{-2} \\ g_{ri}(\rho_i) &= -2f_i - 4c_i\rho_i^{-2} - 6e_i\rho_i^{-4} \end{aligned} \tag{4}$$

$$\begin{aligned} \sigma_{\theta i} &= h_{\theta i}(\rho_i) + g_{\theta i}(\rho_i) \cdot \cos 2\theta \\ h_{\theta i}(\rho_i) &= 2a_i - b_i\rho_i^{-2} \\ g_{\theta i}(\rho_i) &= 2f_i + 12d_i\rho_i^{2} + 6e_i\rho_i^{-4} \end{aligned} \tag{5}$$

$$\begin{aligned} \sigma_{r\theta i} &= h_{r\theta i}(\rho_i) \cdot \sin 2\theta \\ h_{r\theta i}(\rho_i) &= 6d_i\rho_i^{2} + 2f_i - 2c_i\rho_i^{-2} - 6e_i\rho_i^{-4} \end{aligned} \tag{6}$$

$$\begin{aligned} u_i &= h_{ui}(\rho_i) + g_{ui}(\rho_i) \cdot \cos 2\theta \\ h_{ui}(\rho_i) &= -G_i^{-1}\left(a_i\rho_i\alpha_i + \frac{b_i}{2\rho_i}\right) \\ g_{ui}(\rho_i) &= G_i^{-1}\left(e_i\rho_i^{-3} - 2d_i\mu_i\rho_i^{3} - f_i\rho_i - 2c_i\rho_i^{-1}\beta_i\right) \end{aligned} \tag{7}$$

$$\begin{aligned} v_i &= h_{vi}(\rho_i) \cdot \sin 2\theta \\ h_{vi}(\rho_i) &= G_i^{-1}\left(f_i\rho_i + c_i\rho_i^{-1}\alpha_i + e_i\rho_i^{-3} - d_i\rho_i^{3}\gamma_i\right) \end{aligned} \tag{8}$$

where $\alpha_i = 2\mu_i - 1$, $\beta_i = \mu_i - 1$, $\gamma_i = 2\mu_i - 3$, a_i through f_i are unknown coefficients, ρ_i is the non-dimensional radial coordinate, $\rho_i \in [1, k_i]$, and $k_i = \hat{r}_{i+1}/\hat{r}_i$.

The stress boundary conditions of the single-layer model include $\sigma_{r|r=r_i} = p_i$, $\sigma_{r\theta|r=r_i} = q_i$, $\sigma_{r|r=r_{i+1}} = p_{i+1}$, and $\sigma_{r\theta|r=r_{i+1}} = q_{i+1}$. As these stress boundary conditions are applicable to arbitrary angles, they can be solved simultaneously with (4) and (6). The following six equations can therefore be obtained.

$$\begin{aligned} \delta_i &= 2a_i + b_i, \\ \xi_i &= -2f_i - 4c_i - 6e_i \\ \omega_i &= 6d_i + 2f_i - 2c_i - 6e_i, \end{aligned}$$

$$\delta_{i+1} = 2a_i + b_i k_i^{-2}$$
$$\xi_{i+1} = -2f_i - 4c_i k_i^{-2} - 6e_i k_i^{-4} \tag{9}$$

Furthermore, coefficients a_i through f_i can be determined by unifying the group of equations:

$$\begin{aligned}
a_i &= -\frac{1}{2A_i}\left(\delta_i - \delta_{i+1}k_i^2\right)\\
b_i &= k_i^2 A_i^{-1}\left(\delta_i - \delta_{i+1}\right)\\
c_i &= -\frac{k_i^2}{2A_i^3}\left(B_i\xi_i - C_i\xi_{i+1} - k_i^2 D_i\omega_i + D_i\omega_{i+1}\right)\\
d_i &= -\frac{1}{6A_i^3}\left(F_i\xi_i - k_i^2 H_i\xi_{i+1} - I_i\omega_i - k_i^2 J_i\omega_{i+1}\right)\\
e_i &= \frac{k_i^4}{6A_i^3}\left(H_i\xi_i - F_i\xi_{i+1} - 2k_i^2\omega_i + 2\omega_{i+1}\right)\\
f_i &= \frac{1}{2A_i^3}\left(C_i\xi_i - k_i^2 B_i\xi_{i+1} - 2k_i^4\omega_i + 2k_i^2\omega_{i+1}\right)
\end{aligned} \tag{10}$$

where $A_i = k_i^2 - 1, B_i = k_i^4 + k_i^2 + 2, C_i = 2k_i^4 + k_i^2 + 1, D_i = k_i^2 + 1, F_i = 3k_i^2 + 1, H_i = k_i^2 + 3, I_i = 3k_i^2 - 1$, and $J_i = k_i^2 - 3$.

The dimensionless stress and displacement solutions for the single-layer model can be obtained by substituting (10) into (4) - (8).

3.2. Solution for Mechanical Model I. Each individual layer in mechanical model I is normally subjected to one of two limited contact conditions, namely, a complete contact or a smooth contact.

3.2.1. Complete Contact. In the case of complete contact, both the stresses and the displacements at the contact interface are continuous. Hence, according to the compatibility conditions of the displacements, the following equations are valid:

$$u_{j|r=r_{j+1}}\widehat{r}_j = u_{j+1|r=r_{j+1}}\widehat{r}_{j+1} \tag{11}$$
$$v_{j|r=r_{j+1}}\widehat{r}_j = v_{j+1|r=r_{j+1}}\widehat{r}_{j+1} \tag{12}$$

where j=1, 2, 3, …, n-1. Because the above boundary conditions are applicable to arbitrary angles θ, they can be simultaneously determined with (7) - (8). Thus, the following equations can be obtained.

$$h_{uj}\left(r_{j+1}\right)\widehat{r}_j = h_{u(j+1)}\left(r_{j+1}\right)\widehat{r}_{j+1} \tag{13}$$
$$g_{uj}\left(r_{j+1}\right)\widehat{r}_j = g_{u(j+1)}\left(r_{j+1}\right)\widehat{r}_{j+1} \tag{14}$$
$$h_{vj}\left(r_{j+1}\right)\widehat{r}_j = h_{v(j+1)}\left(r_{j+1}\right)\widehat{r}_{j+1} \tag{15}$$

Arranging (13) - (15), we can derive the following formulas:

$$L_j\delta_j + M_j\delta_{j+1} + N_j\delta_{j+2} = 0 \tag{16}$$
$$O_j\xi_j + P_j\omega_j + Q_j\xi_{j+1} + \chi\cdot R_j\omega_{j+1} + S_j\xi_{j+2} + T_j\omega_{j+2} = 0 \tag{17}$$
$$\chi\cdot\left(U_j\xi_j + V_j\omega_j + W_j\xi_{j+1} + X_j\omega_{j+1} + Y_j\xi_{j+2} + Z_j\omega_{j+2}\right) = 0 \tag{18}$$

where $\chi = 1, \Theta_j = G_j\cdot G_{j+1}^{-1}, \varsigma_j = A_j A_{j+1}^{-1}, L_j = \alpha_j - 1$,

$$\begin{aligned}
M_j &= \left(1 - k_j^2\alpha_j\right) - \left(\alpha_{j+1} - k_{j+1}^2\right)\Theta_j\varsigma_j,\\
N_j &= \left(k_{j+1}^2\alpha_{j+1} - k_{j+1}^2\right)\Theta_j\varsigma_j,\\
O_j &= 2F_j\mu_j k_j^2 - 3C_j + 6B_j\beta_j + H_j,\\
P_j &= 2k_j^2\left(3k_j^2 - I_j\mu_j - 3D_j\beta_j - 1\right),\\
Q_j &= \left(3C_{j+1} - 2F_{j+1}\mu_{j+1} - 6B_{j+1}k_{j+1}^2\beta_{j+1} - H_{j+1}k_{j+1}^4\right)\cdot\varsigma_j^3\Theta_j + 3B_j k_j^2 - 2H_j k_j^4\mu_j - 6C_j\beta_j - F_j,\\
R_j &= \left(2I_{j+1}\mu_{j+1} - 6k_{j+1}^4 + 6D_{j+1}k_{j+1}^4\beta_{j+1} + 2k_{j+1}^6\right)\cdot\varsigma_j^3\Theta_j + 6D_j\beta_j - 2k_j^4 J_j\mu_j - 6k_j^2 + 2,\\
S_j &= \varsigma_j^3\Theta_j\left(2H_{j+1}k_{j+1}^2\mu_{j+1} - 3B_{j+1}k_{j+1}^2 + 6C_{j+1}k_{j+1}^2\beta_{j+1} + F_{j+1}k_{j+1}^4\right),\\
T_j &= \left(2k_{j+1}^2 J_{j+1}\mu_{j+1} + 6k_{j+1}^2 - 6k_{j+1}^2 D_{j+1}\beta_{j+1} - 2k_{j+1}^4\right)\cdot\varsigma_j^3\Theta_j,\\
U_j &= 3C_j - 3B_j\alpha_j + H_j + F_j k_j^2\gamma_j,\\
V_j &= 3D_j k_j^2\alpha_j - 6k_j^4 - 2k_j^2 - I_j k_j^2\gamma_j,\\
W_j &= \left(3B_{j+1}k_{j+1}^2\alpha_{j+1} - 3C_{j+1} - H_{j+1}k_{j+1}^4 - F_{j+1}\gamma_{j+1}\right)\cdot\varsigma_j^3\Theta_j + \left(3C_j\alpha_j - 3B_j k_j^2 - F_j - H_j k_j^4\gamma_j\right),\\
X_j &= \left(6k_{j+1}^4 - 3D_{j+1}k_{j+1}^4\alpha_{j+1} + 2k_{j+1}^6 + I_{j+1}\gamma_{j+1}\right)\cdot\varsigma_j^3\cdot\Theta_j + \left(6k_j^2 - 3D_j\alpha_j + 2 - k_j^4 J_j\gamma_j\right),\\
Y_j &= \varsigma_j^3\Theta_j\left(3B_{j+1}k_{j+1}^2 - 3C_{j+1}k_{j+1}^2\alpha_{j+1} + F_{j+1}k_{j+1}^4 + H_{j+1}k_{j+1}^2\gamma_{j+1}\right),\\
Z_j &= \left(3k_{j+1}^2 D_{j+1}\alpha_{j+1} - 6k_{j+1}^2 - 2k_{j+1}^4 + k_{j+1}^2 J_{j+1}\gamma_{j+1}\right)\cdot\varsigma_j^3\Theta_j.
\end{aligned} \tag{19}$$

Table 1: Mechanical parameters of characteristic points on the frozen wall.

$\hat{r}$ (m)	Temperature (°C)	Elastic Modulus (MPa)	Poisson's Ratio
4.2	-12.5	393	0.27
6.8	-25	601	0.22
7.4	-25	601	0.22
10.2	0	219	0.33

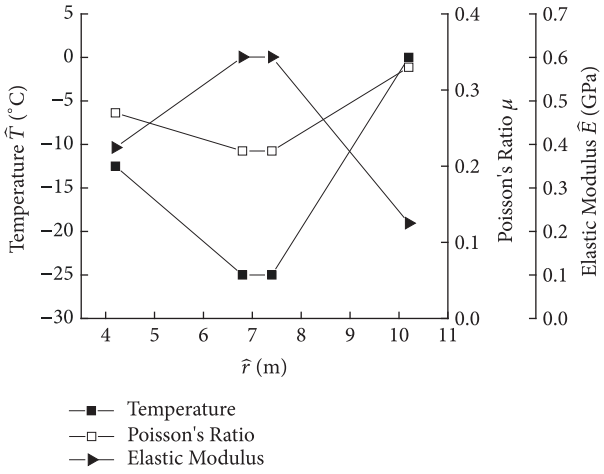

Figure 3: Distributions of the temperature, elastic modulus, and Poisson's ratio with respect to the radial coordinates.

Equations (16)-(18) comprise a $3 \cdot (n\text{-}1)$-degree linear equation group with variables δ_2, ξ_2, ω_2, …, δ_n, ξ_n, and ω_n. These equations can be directly solved using mathematical calculation software. Then, substituting the results into the stress and displacement expressions of mechanical model I, the analytical solutions of stress and displacement for the complete contact condition can be obtained.

3.2.2. Smooth Contact. In the case of smooth contact, the normal stresses and radial displacements at the contact interface are continuous, and the tangential stress is zero.

$$q_{j+1} = 0 \tag{20}$$

Therefore, the undetermined coefficients can be determined using (16)-(18); moreover, under this condition, $\chi = 0$ and $\omega_{j+1} = 0$. Similarly, substituting these coefficients into the stress and displacement expressions of mechanical model I, the analytical solutions of stress and displacement for the smooth contact condition can be obtained.

4. Engineering Example

The distributions of the temperature field, elastic modulus, and Poisson's ratio of a horizontal circular section of a frozen wall at a depth of 150 m are shown in Figure 3. The inner and outer radii of the frozen wall are 4.2 m and 10.2 m, respectively. The parameters of characteristic points within the frozen wall model are summarized in Table 1. The soil gravity is 0.02 MN/m^3. The soil inside the frozen wall is excavated one layer at one time; therefore, the inner edge of the frozen wall is completely unloaded ($p_1 = 0, q_1 = 0$). The external side of the frozen wall is subjected to a formation pressure with a lateral pressure coefficient of $\lambda = 0.65$. The expressions for the stresses in polar coordinates are as follows.

$$\begin{aligned} p_{n+1} &= -\frac{1+\lambda}{2} + \frac{1-\lambda}{2}\cos 2\theta \\ &= -0.825 + 0.175\cos 2\theta \\ q_{n+1} &= -\frac{1-\lambda}{2}\sin 2\theta = -0.175\sin 2\theta \end{aligned} \tag{21}$$

The proposed solution method is used to analyze the distributions of the stress and displacement fields on the frozen wall.

The frozen wall is divided in the radial direction into a cylinder with 55 layers in complete contact according to the temperature distribution. Each layer is assumed to be a homogeneous isotropic elastic body. The flat part of the temperature distribution curve (6.8 m-7.4 m) in the middle of the frozen wall is considered a single layer with a thickness of 0.6 m, an elastic modulus of 601 MPa, and a Poisson's ratio of 0.22. The thickness of each remaining layer is 0.1 m, and the elastic moduli and Poisson's ratio values are obtained by linear interpolating the data shown in Figure 3 and Table 1.

Substituting the values of the physical and mechanical parameters of each layer into (16)-(18), the equations are then solved to obtain the forces and coefficients for every interface. Subsequently, by substituting the results into (4)-(8), the stresses and displacements of each layer can be determined. Thus, the stress and displacement fields of the entire frozen wall can be obtained.

To verify the results of the analytical solution, a finite element model consisting of one-quarter of the ice wall (0-$\pi/2$) in consideration of its symmetry is established. The finite mesh elements are shown in Figure 4, where $\hat{p}_a = 0.02\times150 = 3$ MPa, and the boundary constraint and force conditions are as follows.

(1) Left boundary: sliding support restriction, the displacement in the x-direction being zero

(2) Lower boundary: sliding support restriction, the displacement in the y-direction being zero

(3) Inner boundary: acting loads $\hat{p}_1$ and $\hat{q}_1$

(4) Outer boundary: acting loads $\hat{p}_{56}$ and $\hat{q}_{56}$

Figures 5, 6, and 7 indicate the distributions of the radial stress, radial displacement, and tangential stress, respectively, along both the direction of the minimum earth stress ($\theta = 0$)

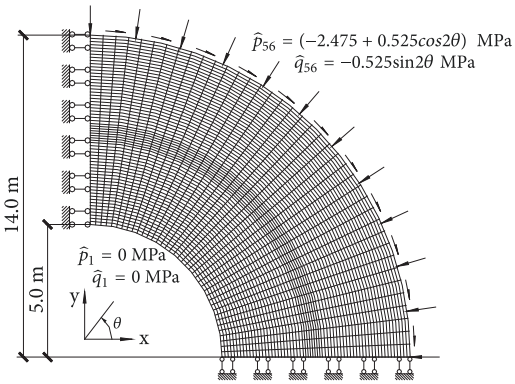

Figure 4: Schematic diagram of the finite element calculation model.

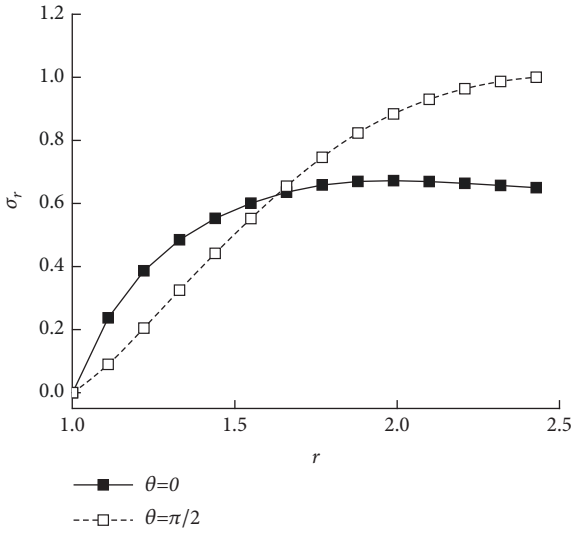

Figure 5: The variation in σ_r in the radial direction.

and the direction of the maximum in situ stress ($\theta = \pi/2$) on the frozen wall. The values of the scattered points represent the results of the finite element calculations, and the curves represent the results of the theoretical calculations.

Figure 5 demonstrates that the radial stress nonlinearly increases in the radial direction and gradually transforms into the in situ stress.

As shown in Figure 6, a slight variation in the radial displacement is observed in the radial direction. The displacement in the direction of the maximum in situ stress ($\theta = \pi/2$) is much greater than that in the direction of the minimum earth stress ($\theta = 0$). This result indicates that the frozen wall experiences larger external expansion in the direction of the maximum in situ stress than in other directions.

Based on Figure 7, where $r = 1$, the tangential stress in the direction of the minimum earth stress ($\theta = 0$) is much higher than that in the direction of the maximum in situ stress ($\theta = \pi/2$). In the former case, the tangential stress decreases nonlinearly in the radial direction; moreover, in the latter case, the tangential stress initially increases nonlinearly and then decreases gradually in the radial direction.

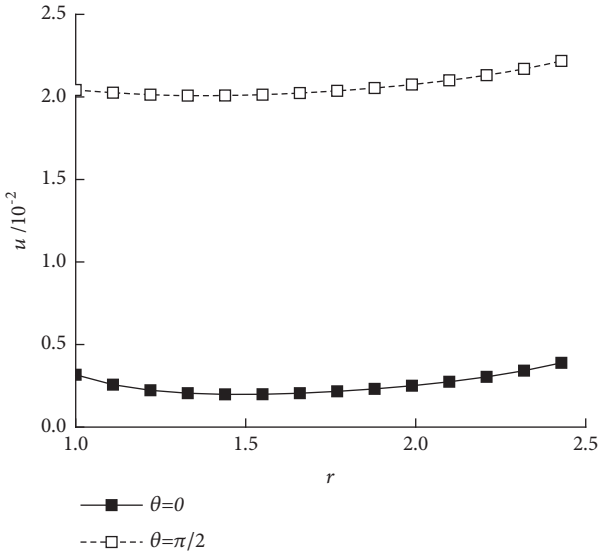

Figure 6: The variation in u in the radial direction.

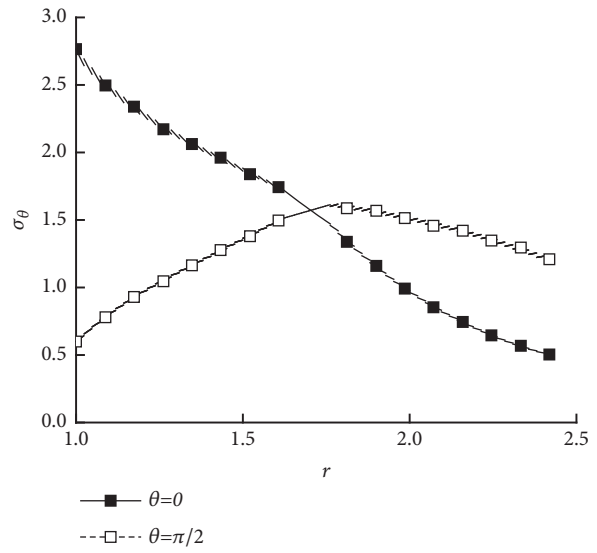

Figure 7: The variation in σ_θ in the radial direction.

Since the results shown in Figures 5, 6, and 7 are consistent with the finite element calculations, the correctness of the theoretical solution is verified.

5. Conclusions

Radial heterogeneous cylinders subjected to asymmetric loads are often encountered in practical engineering. However, it is difficult to obtain the analytical solutions of the corresponding stress and displacement. Although previous studies have developed various solutions to this problem, those solutions are relatively complex and do not consider the comprehensive effects of different loads. Consequently, this paper proposes a stress and displacement solution method for the plane strain on a radial heterogeneous cylinder with inner and outer surfaces subjected to uneven normal and

tangential pressures under two types of contact conditions (i.e., complete contact and smooth contact) based on the theory of elastic mechanics. In addition, a group of linear equations ((16)-(18)) is derived, through which the analytical solution for a radial heterogeneous cylinder under a non-uniform load can be obtained. Then, a finite element model of a horizontal circular frozen wall subjected to an uneven formation pressure is constructed to verify the correctness of the analytical solution, and the results indicate that the analytical solution is relatively universal and can be applied to realistic engineering applications involving cylindrical structures. Accordingly, the study provides a theoretical basis for the stress state analysis, stability evaluation, and structural design of cylindrical structures, all of which have great significance in practical engineering.

Data Availability

The data used to support the findings of this study are available from the corresponding author upon request.

Conflicts of Interest

The authors declare that there are no conflicts of interest regarding the publication of this paper.

Acknowledgments

This work was financially supported by the National Hightech R&D Program of China (86-3 Program; no. 2012AA06A401) and the National Natural Science Foundation of China (nos. 41472224 and 41501075).

References

[1] G. Lamé and B. Clapeyron, "Mémoire sur l'équilibre intérieur des corps solides homogènes," *Journal für die reine und Angewandte Mathematik*, vol. 7, pp. 145–169, 1831.

[2] Ъ. Г. Галеркин, "Напряженное состояние цилиндрической трубы в упругой среде," труды липс, Russia, 100, 1929.

[3] D. C. Liu and Y. Zhao, "Stability analysis of cylindrical shells under external pressures by half analytical finite element method," *Engineering Mechanics*, vol. 9, no. 1, pp. 104–114, 1992.

[4] A. P. Parker, "Autofrettage of open-end tubes-pressures, stresses, strains, and code comparisons," *Journal of Pressure Vessel Technology, Transactions of the ASME*, vol. 123, no. 3, pp. 271–281, 2001.

[5] M. Ghannad and M. Z. Nejad, "Elastic analysis of heterogeneous thick cylinders subjected to internal or external pressure using shear deformation theory," *Acta Polytechnica Hungarica*, vol. 9, no. 6, pp. 117–136, 2012.

[6] H. Jahed, B. Farshi, and M. Karimi, "Optimum autofrettage and shrink-fit combination in multi-layer cylinders," *Journal of Pressure Vessel Technology, Transactions of the ASME*, vol. 128, no. 2, pp. 196–200, 2006.

[7] M. Schwartz, *New Materials, Processes, And Methods Technology*, Boca Raton: CRC Press, 2005.

[8] Y. L. J. Song and Z. M. Zhang, *Functionally Graded Mechanics*, Tsinghua University Press, China, 2003.

[9] L. M. Smith, *Engineering with Clad Steel*, Technical series no. 10064, The Nickel Institute, Brussels, Belgium, 2nd edition, 2012.

[10] K. Vedeld, H. Osnes, and O. Fyrileiv, "Analytical expressions for stress distributions in lined pipes: Axial stress and contact pressure interaction," *Marine Structures*, vol. 26, no. 1, pp. 1–26, 2012.

[11] Z. Shi, T. Zhang, and H. Xiang, "Exact solutions of heterogeneous elastic hollow cylinders," *Composite Structures*, vol. 79, no. 1, pp. 140–147, 2007.

[12] H. A. Sollund, K. Vedeld, and J. Hellesland, "Efficient analytical solutions for heated and pressurized multi-layer cylinders," *Ocean Engineering*, vol. 92, pp. 285–295, 2014.

[13] C. O. Horgan and A. M. Chan, "The pressurized hollow cylinder or disk problem for functionally graded isotropic linearly elastic materials," *Journal of Elasticity: The Physical and Mathematical Science of Solids*, vol. 55, no. 1, pp. 43–59, 1999.

[14] A. Lu and N. Zhang, "Inversion of functionally graded materials to improve the elastic ultimate bearing capacity of thick-walled hollow cylinder," *Advanced Materials Research*, vol. 378-379, pp. 116–120, 2012.

[15] A.-Z. Lu, N. Zhang, Y.-Q. Xu, and P. Cui, "Stress-displacement solution for a lined vertical borehole due to non-axisymmetric in situ stresses," *International Journal of Rock Mechanics and Mining Sciences*, vol. 57, pp. 64–74, 2013.

[16] C. Carranza-Torres, B. Rysdahl, and M. Kasim, "On the elastic analysis of a circular lined tunnel considering the delayed installation of the support," *International Journal of Rock Mechanics and Mining Sciences*, vol. 61, pp. 57–85, 2013.

[17] Y. Wang and W. Yang, "Elastic stress analysis on circular frozen wall in bi-directional unequal ground stress field under unloading condition," *Caikuang yu Anquan Gongcheng Xuebao/Journal of Mining and Safety Engineering*, vol. 33, no. 3, pp. 486–493, 2016.

[18] E. Detournay and C. M. St. John, "Design charts for a deep circular tunnel under non-uniform loading," *Rock Mechanics and Rock Engineering*, vol. 21, no. 2, pp. 119–137, 1988.

[19] W. Ming-Bin and L. Shu-Chai, "A complex variable solution for stress and displacement field around a lined circular tunnel at great depth," *International Journal for Numerical and Analytical Methods in Geomechanics*, vol. 33, no. 7, pp. 939–951, 2009.

[20] Q.-L. Wu, A.-Z. Lü, Y.-T. Gao, S.-C. Wu, and N. Zhang, "Stress analytical solution for plane problem of a double-layered thick-walled cylinder subjected to a type of non-uniform distributed pressure," *Journal of Central South University*, vol. 21, no. 5, pp. 2074–2082, 2014.

[21] C.-L. Hu, J. Xu, and C. Xiao, "Stress analysis of thick cylinder supporting structure under eccentric load," *Yantu Lixue/Rock and Soil Mechanics*, vol. 33, no. 7, pp. 2117–2121, 2012.

[22] J. H. Nester and D. R. Jenkins, "Resistances to Failure of Oil-well Casing Subjected to Non-uniform Transverse Loading," *Drilling and Production Practice*, vol. 55, pp. 374–378, 1955.

[23] F. Khalaf and U. Cairo, "Increasing Casing Collapse Resistance Against Salt-Induced Loads," in *Proceedings of the Middle East Oil Technical Conference and Exhibition*, vol. 13712, pp. 259–264, 1985.

[24] A. El-Sayed, F. Khalaf, and U. Cairo, "Resistance of Cemented Concentric Casing Strings Under Nonuniform Loading," *SPE Drilling Engineering*, vol. 17927, no. 01, pp. 59–64, 2013.

[25] S. P. Timoshenko and J. N. Goodier, *Theory of elasticity*, McGraw-Hill, New York, NY, USA, 1970.

[26] N. Muskhelishvili, *Some Basic Problems of the Mathematical Theory of Elasticity*, Noordhoof Ltd., Groningen, The Netherlands, 1963.

[27] J. B. Greenberg and Y. Stavsky, "Buckling of composite orthotropic cylindrical shells under non-uniform axial loads," *Composite Structures*, vol. 30, no. 4, pp. 399–406, 1995.

[28] A. Behravan Rad, "Thermo-elastic analysis of functionally graded circular plates resting on a gradient hybrid foundation," *Applied Mathematics and Computation*, vol. 256, pp. 276–298, 2015.

[29] K. M. Liew, S. Kitipornchai, X. Z. Zhang, and C. W. Lim, "Analysis of the thermal stress behaviour of functionally graded hollow circular cylinders," *International Journal of Solids and Structures*, vol. 40, no. 10, pp. 2355–2380, 2003.

[30] R. C. Batra and G. J. Nie, "Analytical solutions for functionally graded incompressible eccentric and non-axisymmetrically loaded circular cylinders," *Composite Structures*, vol. 92, no. 5, pp. 1229–1245, 2010.

[31] H. Li and Y. Liu, "Functionally graded hollow cylinders with arbitrary varying material properties under nonaxisymmetric loads," *Mechanics Research Communications*, vol. 55, pp. 1–9, 2014.